

PARFAIT: GNSS-R coastal altimetry

M. Caparrini, L. Ruffini, G. Ruffini

Starlab, C. de l'Observatori Fabra s/n, 08035 Barcelona, Spain, <http://starlab.es>.

Abstract

GNSS-R signals contain a coherent and an incoherent component. A new algorithm for coherent phase altimetry over rough ocean surfaces, called PARFAIT, has been developed and implemented in Starlab's STARLIGHT¹ GNSS-R software package. In this paper we report our extraction and analysis of the coherent component of L1 GPS-R signals collected during the ESTEC Bridge 2 experimental campaign using this technique. The altimetric results have been compared with a GPS-buoy calibrated tide model with a resulting precision of the order 1 cm.

Keywords: Passive radar, GNSS, GPS, Galileo, GNSS-R, GPS-R, altimetry, PARIS, PIP, PARFAIT, coastal applications.

1. Introduction

Specular reflections dominate medium to short wavelength electromagnetic forward scattering on the ocean, examples of which include GNSS and solar reflections. As reported in [23], during the last decade many GPS-R (Global Positioning System Reflections) experimental campaigns have now been successfully carried out. A partial and surely incomplete list is provided in Table 1. In this paper we focus on the potential of GNSS-R (Global Navigation Satellite System Reflections) for altimetric coastal applications. The techniques developed, however, can also be implemented in other scenarios (airborne, spaceborne).

The specularly scattered field is composed of a coherent component and a random, Hoyt-distributed component [2]. When the surface is very rough, the latter becomes incoherent and the former becomes very small. In fact, if the surface height distribution is normal with deviation σ_ζ , then

$$\langle r^2 \rangle \sim n^2 e^{-(4\pi\sigma_\zeta \cos\theta/\lambda)^2} + \quad (1)$$

$$n(1 - e^{-(4\pi\sigma_\zeta \cos\theta/\lambda)^2}),$$

where $\langle r^2 \rangle$ is the power average, n is the number of scatterers, λ the EM wavelength and θ the local incidence angle [23, 24].

GNSS-R signals thus contain a coherent and an incoherent component. In companion papers we discuss the analysis of the incoherent component for sea state monitoring [15, 25]

and for code altimetry [27]. Here we present a new approach for the extraction and analysis of the coherent component of GNSS reflected signals to perform phase altimetry.

The data discussed here was collected by ESA/ESTEC during the Bridge-2 experiment. The experiment aimed at gathering direct and reflected GPS signals from antennas located about 18 m above the mean sea level of an Estuary in the North sea of Holland. For more information on the experimental setup, the reader is directed to [21].

This paper is structured as follows:

- Discussion on coherence properties of reflected signals and their use for phase altimetry.
- Analysis of the direct and reflected signals and EM field extraction.
- Implementation of PARFAIT altimetry.
- Comparison with other data and discussion of the altimetric results.

2. The complex field

The importance of retrieving the coherent part of the EM field backscattered by the sea surface stems from its altimetric content. Measuring the phase of the coherent component allows for accurately estimating the delay of the reflected signal with respect to the direct one, i.e., for estimation of the temporal

Main Author	Inst.	Date	Notes
Garrison [11]	JPL	1996	A normal GPS receiver was used. Demonstrated reception/tracking of reflected signals over relatively calm waters. Concluded that more complex receiver is needed.
Martin-Neira [18, 3] Caparrini	ESA	1997	GNSS-R PARIS altimetric experiment from a Zeeland bridge. C/A code used for correlation leading to an altimetric accuracy in the order of 3 meters after 1 second (1% of the chip length).
Garrison [13]	JPL	1997	Widening of correlation function in rough seas demonstrated. Application for sea state from air.
Komjathy [16]	CCAR	1998	Aircraft experiments, 3-5 km altitude.
LaBrecque [17]	NASA	1998	The first spaceborne observation of GPS signals reflected from the ocean surface.
Cardellach [9, 12] Ruffini Garrison	IIEC	1999	Balloon experiment. Successful detection of reflected signals at 38 km of height with low gain antenna. Sea surface winds retrieved with ~ 2 m/s error.
Cardellach [5] Ruffini	IIEC	1999	First ESA aircraft experiment. Some signals detected, DDM produced, but experiment failed due to hardware problems.
Armatys [1]	CCAR	2000	Wind speed and directions obtained from reflected GPS signals are compared to the Sea-Winds scatterometer on-board QuikSCAT.
Garrison [10]	JPL	2000	With GPS-R airborne data, retrieval of the wind speed with a bias of less than 0.1 m/s and with a standard deviation of 1.3 m/s.
Zavorotny [28]	CCAR	2000	Fundamental theoretical work. Comparison of experimental and theoretical waveforms.
Zuffada [29]	JPL	2000	Lakeside experiment, with an almost flat surface (no roughness). Centimetric phase altimetry.
Martin-Neira, [26] Ruffini, Serra, Colmenarejo	ESA	2000	The pond experiment was designed to test some key issues in the PARIS Interferometric Processor (PIP) concept. The PIP concept is based on the use of dual-frequency carrier measurements to exploit the correlations in the scattered signals at similar frequencies.
Ruffini [4] Caparrini	Starlab IIEC	2001	GPS-R L1 data collected from the Casablanca drilling platform by IIEC has been analysed at Starlab.
Martin-Neira [20]	ESA	2001	The experimental campaign which is the object of this work.
Cardellach [8, 7, 6, 14] Starlab Team	IIEC/ Starlab	2001	GPS-R data collection from airborne platform. Campaign performed within the ESA/ESTEC project "PARIS Alpha". Data processed under ESA/ESTEC projects "PARIS Alpha" and "OPPSCAT 2".
Starlab [15, 27] Team	Starlab	2002	GPS-R data collection from airborne platform. Retrieval of altimetric profile matching Jason-1. (ESA/ESTEC "PARIS Gamma")
Starlab [25] Team	Starlab	2003	GPS-R data collection from Barcelona Harbour (HOPE campaign, Starlab Oceanpal project).

lapse. This is the essential measurement for altimetry [26].

In order to collect the complex EM field, the complex signal is generated from the real one. Although this operation is often performed by the receiver front-end, in the Bridge-2 experiment only the in-phase component of the signal was sampled at high frequency and stored on digital tape. The quadrature component was generated afterwards. The process is illustrated in Figure (1). We can then represent the direct signal received at the antenna input² as

$$S_d(t) = A_d \cdot C(t) \cdot D(t) \cdot e^{i(\omega_{L1} + \omega_d)t} + \eta_d, \quad (2)$$

where A_d is the direct signal amplitude, $C(t)$ represents the C/A code, $D(t)$ the navigation code, ω_{L1} the L1 carrier frequency, ω_d the Doppler frequency offset, and η_d (thermal) noise. The reflected signal at low altitudes can be modelled by

$$S_r(t) = C(t) \cdot D(t) \cdot e^{i(\omega_{L1} + \omega_d)t}. \quad (3)$$

$$\left(A_r \cdot e^{2\pi i \mathcal{L}/\lambda} + O(t) \right) + \eta_r,$$

where A_r is the reflected signal mean amplitude, $O(t)$ represents the perturbation due to ocean motion and \mathcal{L} the reflected signal extra path length. In coastal applications $O(t)$ is a relatively slowly varying quantity with zero mean, while \mathcal{L} , which contains the geophysical tide signal, can be considered effectively frozen during correlation processing.

After modulation with a local oscillator of frequency $\omega_{L1} - \omega_{IF}$ and low-pass filtering, the signal will have a residual carrier at $\omega_d + \omega_{IF}$. This signal is mixed with a phasor at frequency $\omega_{IF} + \tilde{\omega}_d$, where $\tilde{\omega}_d$ is an estimate of the Doppler frequency for the satellite under investigation, and finally low-pass filtered.

With the assumption that the navigation bit is constant during the integration time (which is correct if the correlation is bit-aligned and the coherent integration time T_E is less than 20 ms), and considering that during an integration time interval the value of $\Delta\omega_d$ is constant, the complex p -th sample of the correlation coefficient for the direct signal

writes

$$C_p \sim \frac{1}{2} A_d D_k R_p e^{-i\Delta\omega_{d_p} T_E (p-1)} \cdot e^{-i\Delta\omega_{d_p} \frac{T_s}{2}} \frac{\sin\left(\frac{\Delta\omega_{d_p} T_E}{2}\right)}{\sin\left(\frac{\Delta\omega_{d_p} T_s}{2}\right)}, \quad (4)$$

where T_s is the sampling interval and R_p the corresponding correlation coefficient function. For the reflected signal we can write an equivalent expression, modulated by the slowly varying phasor $A_r \cdot \exp(2\pi i \mathcal{L}/\lambda) + O(t)$. For coastal applications we can assume there will be little filtering of this quantity by the coherent integration process, as the ocean moves slowly compared to coherent integration times (a few ms).

In the case of the direct signal, we can easily track the carrier phase. To this end, the delta-phases obtainable from equation (4) can be accumulated using

$$\begin{aligned} \phi_{p+1} - \phi_p &= \\ &= \text{Im} \left(\log \frac{C_{p+1}}{C_p} \right) = -\Delta\omega_{d_p} T_E. \end{aligned} \quad (5)$$

This equation holds while $\Delta\omega_{d_{p+1}} \approx \Delta\omega_{d_p}$. This is a good approximation, since the time during which this variation is measured is the coherent integration time.

The main advantage of using this algorithm for phase tracking is that, due to its differencing nature, it allows for easy detection of the navigation bit π radians phase change.

Figures 2 to 8, which illustrate these concepts, refer to the processing of another set of GPS-R data—collected during the Casablanca oil platform Experiment. This Repsol owned drilling platform is about 40 km off the coast of Tarragona, Spain ($40^\circ 43' 4'' N$, $1^\circ 21' 34'' E$). The measurement campaign took place on March 14th, 2000.

In Figure 2, the histogram of the delta-phases is shown. The x-axis represents cycles and the y-axis is in arbitrary units. Most δ -phase values are clearly concentrated around zero. Other values gather just before $\pm\pi$. These values represent in fact *small* values to which $\pm\pi$ radians have been added on occurrence of a navigation bit transition.

In Figure 3, the direct signal phase with and without navigation bit correction is plotted. In Figure 4, the phase for the (navi-

²This contains only the C/A code part. The P code component can be neglected thanks to the subsequent correlation of the signal with replicas of the C/A code—the two codes are orthogonal.

gation bit corrected) direct and reflected signals is shown. The effect of the reflection on the sea surface is clearly visible in the large variations present in Figure 4(b) with respect to Figure 4(a). In Figure 5 and 6, the amplitude magnitude and the complex vector of the direct and reflected fields, respectively, are shown. In Figure 8, a simulation of the L1 GPS complex field phasor *dustball* after reflection, akin to the one in Figure 6(b), is shown. The simulation parameters have been chosen to match the Casablanca experiment sea state. Those were reported as a “quite calm sea with a gentle breeze”, with SWH of about 0.7 m as measured by a nearby buoy.

3. The PARFAIT approach

In general, the altimetric information content in the PARIS interferometric field phase will be very difficult to use. This is due to the impact of the incoherent component in the reflected signals. The incoherent component causes fading and winding.

On the one hand, at a practical level, fading events will prevent stable phase tracking of the complex field. Even if as in the Bridge-2 experiment the sea surface is relatively smooth and fading events are not so frequent, a single event can severely complicate the use of phase information if countermeasures are not taken. In general, however, the reflected field will fade very often. As discussed in [21], it is possible to inject in the system (during a fading event) a model-based phase to “glue” the phase history, but this approach will in general necessitate the input of too much model information into the data in rough sea conditions.

More importantly, as explained in the previous section, the reflected field incoherent component will cause arbitrary winding of the field phasor. This means that the reflected unwrapped phase, unlike the direct one, cannot be directly used for ranging. Indeed, as we have shown in previous work [26], the reflected field accumulated phase will generally wander around the complex plane, travelling to different winding number kingdoms, *even in the absence of fadings* (see Figure 7). That is to say, even if a very high SNR system is devised to get around the problem of field fadings, the interferometric unwrapped phase will not be directly usable for ranging. Unlike the prob-

lem of fadings, this is a fundamental issue, not a practical one.

An approach discussed in [26, 19], PIP³, involves the use of multiple frequencies for the synthesis of a longer wavelength which will be more immune to fadings. Here we discuss another approach, PARFAIT⁴, which is in fact complementary to PIP.

In the PARFAIT approach, we begin by noting that although the reflected field unwrapped phase carries no ranging information, this need not be a fundamental problem. What is needed is the coherent *geophysical* field component in the signals, which is near zero frequency in comparison with the others—a sort of average field. This average field is just the coherent component in the reflected signals after downconversion. With this in mind, PARFAIT consists of the three steps described next.

The first practical step to extract the coherent part is to work with the interferometric field, the ratio for reflected versus direct complex field. This has the advantage of error cancellation, e.g., in Doppler matching of the incoming signals, and of depending only on the lapse.

The second step is to “counter-rotate” the interferometric field using an a-priori model of the reflection process.

The third step is filtering the resulting counter-rotated interferometric complex field to finally extract the coherent phase for estimation of the carrier lapse phase. Counter-rotation allows for longer filtering times. These are fundamental to extract the coherent component, which decays exponentially with the square of sea surface standard deviation (sea state) over effective wavelength (the wavelength divided by the sine of satellite elevation).

Finally, the phase lapse information obtained from the counter-rotated, averaged, complex interferometric field is used for altimetry.

This new approach to PARIS altimetry is described in more detail in the following sections. As we discuss, it has proven to be a very robust and precise processing method.

³PARIS Interferometric Processor.

⁴PARFAIT stands for PARis Filtered-field AltImetric Tracking.

4. PARFAIT processing of the Bridge 2 dataset

At low altitudes, simple geometrical considerations lead to the following equation relating the height of the receiver over the reflecting surface (considering the same height for the upward looking antenna and for the downward looking antenna) with the lapse—the measured delay measured between the direct and reflected GNSS signals:

$$\mathcal{L}_P(t) = c\Delta\tau_P(t) = 2h(t) \cdot \sin(\epsilon_P(t)) + b, \quad (6)$$

where $\mathcal{L}_P(t)$ is the lapse in meters at time t , c is the speed of light, $\Delta\tau_P(t)$ is the temporal lapse in seconds, $h(t)$ is the height of the bridge, $\epsilon_P(t)$ is the elevation of the GPS satellite with a specific PRN number P , and b is the hardware-induced delay bias, considered to be a common constant in time. A first estimation of the height of the receiver can easily be performed through a linear fit of the lapse with respect to the sine of the elevation angle of each satellite.

In phase processing, the lapse is measured only up to an integer number of cycles N . Equation (6) must be rewritten as follows

$$\mathcal{L}_P^c(t) = 2h(t) \cdot \sin(\epsilon_p(t)) + b + N_p\lambda, \quad (7)$$

with $\mathcal{L}_P^c(t)$ is the carrier lapse in meters and λ is the carrier (L1) wavelength. In other words, the equation for each satellite contains an additional unknown parameter, N_P . In order to use all the satellites for one height estimation, it becomes necessary to estimate also N_P , i.e. to solve the ambiguity problem.

In order to solve the estimation problem, a minimization search is carried out for all these parameters: h and b (as real constants) and N_P (as integers).

However, as discussed, the interferometric field should be first filtered to extract its coherent component. Filtering should be long enough to extract the coherent component but short enough to keep the geophysical signals of interest pass through.

This means that the geophysical coherent component we are after should not change for more than a small fraction of a cycle during the time duration of the filter. The maximal allowable time thus depends on the elevation angle and rate of change of elevation of the satellite and, just slightly, on the tide motion. In the case of interest, it turns out the maximum filtering time should be around

10 seconds. In other words, in 10 seconds, at least for one satellite, the coherent interferometric phase changes by more than $\frac{\pi}{2}$ radians. With this filter length it is not possible to separate coherent and incoherent components of the field, and fading events are not completely eliminated. However, a realistic estimation of the bridge height (and bias) does become possible.

As mentioned, to extract the coherent component a longer averaging period should be used. To this end, we first counter-rotate the interferometric field using a first guess of the bridge height, as we now explain in more detail.

After downconversion and despreading, we can express the reflected complex field as a sum of the coherent and incoherent components,

$$E(t) = A_r e^{i\mathcal{L}(t)/\lambda} + O(t). \quad (8)$$

Now consider that we have a first guess for the height and bias parameters, i.e., a model for the lapse \mathcal{L}_m . This model is used to counter-rotate the field:

$$\begin{aligned} E^{cc}(t) &= E(t)/E_m(t) \\ &= A_r e^{2i\delta h(t) \sin(\epsilon_p(t)) + i\delta b} + O'(t). \end{aligned} \quad (9)$$

Clearly, the phase of the coherent field in equation (9) will now vary much slower than the phase of the original reflected field as a function of the elevation (and therefore time). This allows for a longer filtering time, and the extraction of the coherent component of the signal (recall that $O(t)$ has zero mean).

The equation which relates the counter-rotated phase lapse between direct and reflected signal, the satellite elevations and the δh (i.e. the error between the first guess of the bridge height and the real value) is

$$\mathcal{L}_P^c(t) = 2\delta h(t) \cdot \sin(\epsilon_P(t)) + \delta N_P\lambda + \delta b. \quad (10)$$

This is the new equation to be used to fit the lapse versus sine of elevation straight line and infer the height offset of the bridge and bias (with respect to the first guess used to counter-rotate the field).

In order to solve the ambiguity problem, a search is performed in the space of the integer n-tuples and the one that produces the linear fit with smallest residue is selected. It is important to point out that the n-tuple search space is drastically reduced by the prior

field counter-rotation. For example, if the guess is within \pm half meter, the n-tuple subspace to be scanned can be limited to those n-tuples whose components belong to the interval $[-3, 3]$, centered on the first guess of the n-tuple, as obtained from a real (as opposed to integer) ambiguity resolution.

Another way to reduce the cardinality of the subspace of the n-tuples to check is to consider that satellites with similar elevation angles cannot have very different integer ambiguities.

5. Results and comparison

The PARFAIT algorithm described in the previous section, has been used to analyze the first 10 minutes of the Bridge-2 data, Part A1 and to the first 10 minutes of Part A2. The following steps have been performed accordingly in batches of 2 minutes:

- The EM fields, direct and reflected, have been computed through the usual correlation process.
- The complex interferometric field has been counter-rotated (Equation (9)).
- The counter-rotated field has been filtered using a 30 s window.
- The phase of the interferometric, counter-rotated and filtered field has been unwrapped.
- For every possible set of values of the ambiguities N_P , a straight line has been interpolated to the phase histories (one for each visible satellite) against the elevation angle (Equation (10)). The best fit has been identified.

The analysis has been carried out for almost⁵ all visible satellites (see Table 2 and Figure 10). The phase histories are shown in Figure 11(a). A straight line has been fit through these phase histories, against the sine of the satellite elevation angle (Figure 11(b)).

This fitted line gives an estimation of the bridge height of 18.61 m, a hardware bias of -0.81 m and, as first guess for the n-tuple that solves the ambiguity problem, the values $[0\ 0\ 1\ 1\ 2\ 3]$. Now, a search in a subset of \mathcal{I}^6 is carried out to minimise the residuals of the fit in the space of the n-tuples of integers.

The subspace considered is the one spanned by all the combination of integers between ± 3 around the first guess. The result is the n-tuple $[0\ 0\ 2\ 2\ 4\ 5]$ which gives a bridge height estimation of 18.82 m and an instrumental bias of -0.45 m.

This procedure has been implemented with data from the first 10 minutes of Part A1 and A2 of the Bridge-2 experiment. The results are reported in Table 3 and in Figure 12 for Part A1 and in Table 4 and in Figure 13 for Part A2.

Fitting both parts to the tide curve, i.e. choosing the bias that minimizes the standard deviation of the data to the available tide “ground truth”, leads to an altimetry bias of 40 cm and a standard deviation of less than 1 cm. This bias could have an origin in the ground “truth”, due either to an error in the determination of the absolute value of the height of the bridge performed using the GPS buoy available data (only a few seconds, which may have caused ambiguity resolution problems) or, partially, to some anomalies in the water mass flow in the vicinity of the bridge structures.

Moreover, considering also that the tide dynamics measured below the bridge may be delayed with respect to the place where the tide was measured, the best fit (over both bias and delay) is obtained with a delay of 1 minutes and 37 seconds with respect to the time of the tide data collection and with a bias of 40 cm. The standard deviation of the fitted data with respect to the tide curve is in this case of 0.3 cm.

To summarize, the proposed approach to PARIS altimetry, the PARFAIT technique, leads a very precise estimation of the tide,

- without the need to insert any kind of model for the phase of the reflected signal during fadings,
- without rejecting too many visible satellites because of their poor SNR and/or frequent fadings.

Finally, we note that this technique is directly applicable for PARIS phase processing from air and spaceborne applications, as long as a suitable model for the lapse phase can be constructed. This will be the subject of future work.

⁵Satellites outside the *Zeeland Mask* [20, 21] are not considered (see also the caption in Figure 10).

PRN	elevation	mean SNR (direct)	mean SNR (reflected)
14	17°	29.4 dB	25.0 dB
25	17°	32.0 dB	25.8 dB
1	30°	31.2 dB	24.6 dB
7	38°	33.2 dB	29.4 dB
11	62°	34.0 dB	29.4 dB
20	78°	30.4 dB	26.6 dB

Table 2: Visible satellites, their elevation in degrees, the 10 ms coherent integration mean SNR_{dB_w} ($20 \log_{10}[\text{peak-grass/grass correlation coefficient}]$) for the direct and the reflected signal.

time (minutes from start)	instrumental bias [cm]	bridge height estimation [m]	assumed ground truth [m]	difference [cm]
1	-0.45	18.83	18.44	39.71
3	-0.45	18.82	18.42	39.63
5	-0.46	18.81	18.41	40.19
7	-0.45	18.79	18.39	40.21
9	-0.26	18.78	18.38	39.83

Table 3: Results of the bridge height estimation during the first 10 minutes of the Part A1 data.

Acknowledgements

The authors wish to thank Manuel Martin-Neira (Technical Manager of the ESA/ESTEC Contract No. 14285/85/nl/pb under which this work was carried out) and Maria Belmonte (ESA/ESTEC) for useful discussions and real collaboration. We also thank the other partners in the project, especially GMV for the GPS buoy data analysis.

All Starlab authors have contributed significantly; the Starlab author list has been ordered randomly.

References

- [1] M. Armatys, A. Komjathy, P. Axelrad, and S. Katzberg. A comparison of GPS and scatterometry sensing of ocean wind speed and direction. In *Proc. IEEE IGARSS, Honolulu, HA*, 2000.
- [2] P. Beckmann and A. Spizzichino. *The scattering of electromagnetic waves from rough surfaces*. 1963.
- [3] M. Caparrini. Using reflected GNSS signals to estimate surface features over wide ocean areas. Technical Report EWP 2003, ESA report, December 1998.
- [4] M. Caparrini and G. Ruffini. Casablanca data processing. Starlab "Knowledge Nugget" kn-0111-001, 2001.
- [5] E. Cardellach, J.M. Aparicio, A. Rius, J.S., and J. Torrobella. Application of the PARIS concept to transoceanic aircraft remote sensing. Technical report, 2001. PARIS Alpha WP5200 - ESA Contract 14285/85/NL/PB.
- [6] E. Cardellach and A. Rius. Comparison of PAFEX estimates with ground truth. Technical report, IEEC, 2002. WP210 of OPPSCAT 2 Project - ESA Contract RFQ/3-10120/01/NL/SF.
- [7] E. Cardellach and A. Rius. Inversion of PAFEX data with elfouhaily's technique. Technical report, IEEC, 2002. WP205 of OPPSCAT 2 Project - ESA Contract RFQ/3-10120/01/NL/SF.
- [8] E. Cardellach and A. Rius. Preprocessing of PAFEX data. Technical report, IEEC, 2002. WP120 of OPPSCAT 2 Project - ESA Contract RFQ/3-10120/01/NL/SF.
- [9] E. Cardellach, G. Ruffini, D. Pino, A. Rius, A. Komjathy, and J. Garrison. Mediterranean balloon experiment: GPS reflection for wind speed retrieval from

time (minutes from start)	instrumental bias [cm]	bridge height estimation [m]	assumed ground truth [m]	difference [cm]
1	-0.27	17.54	17.11	42.34
3	-0.28	17.52	17.08	42.36
5	-0.26	17.47	17.04	42.52
7	-0.08	17.44	17.02	41.95
9	-0.08	17.41	16.98	42.71

Table 4: Results of the bridge height estimation during the first 10 minutes of the Part A2 data.

- the stratosphere. *To appear in Remote Sensing of Environment*, 2003.
- [10] J.L. Garrison, S. Katzberg, V. Zavorotny, and D. Masters. Comparison of sea surface wind speed estimates from reflected GPS signals with buoy measurements. In *Proc. IEEE IGARSS, Honolulu, HA*, 2000.
- [11] J.L. Garrison, S.J. Katzberg, and C.T. Howell. Detection of ocean reflected GPS signals: theory and experiment. In *IEEE Southeaston '97*. IEEE, April 1997.
- [12] J.L. Garrison, G. Ruffini, A. Rius, E. Cardellach, D. Masters, M. Armatys, and V.U. Zavorotny. Preliminary results from the GPSR mediterranean balloon experiment (GPSR-MEBEX). In *Proceedings of ERIM 2000*, Charleston, South Carolina, USA, May 2000.
- [13] L. Garrison, S. Katzberg, and M. Hill. Effect of sea roughness on bistatically scattered range coded signals from the GPS. *Geophysical Research Letters*, 25:2257–2260, 1998.
- [14] O. Germain and G. Ruffini. Least square inversion of PAFEX data. Technical report, Starlab, 2002. WP200 of OPP-SCAT 2 Project - ESA Contract RFQ/3-10120/01/NL/SF.
- [15] O. Germain, G. Ruffini, F. Soulat, M. Caparrini, B. Chapron, and P. Silvestrin. The GNSS-R Eddy Experiment II: L-band and optical speculometry for directional sea-roughness retrieval from low altitude aircraft. In *Proceedings of the 2003 Workshop on Oceanography with GNSS-R*. Starlab, July 2003.
- [16] A. Komjathy. GPS surface reflection using aircraft data: analysis and results. In *Proceedings of the GPS surface reflection workshop*. Goddard Space Flight Center, July 1998.
- [17] J. LaBrecque, S.T. Lowe, L.E. Young, E.R. Caro, L.J. Romans, and S.C. Wu. The first spaceborne observation of GPS signals reflected from the ocean surface. In *Proceedings IDS workshop*. JPL, December 1998.
- [18] M. Martín-Neira, M. Caparrini, J. Font-Rossello, S. Lannelongue, and C. Serra. The PARIS concept: An experimental demonstration of sea surface altimetry using GPS reflected signals. *IEEE Transactions on Geoscience and Remote Sensing*, 39:142–150, 2001.
- [19] M. Martín-Neira, P. Colmenarejo, and G. Ruffini. Ocean altimetry interferometric method and device using gnss signals, April 2003. U.S. Patent No. 6,559,165 B2.
- [20] M. Belmonte Rivas and M. Martín-Neira. GNSS reflections: First altimetry products from bridge-2 field campaign. In *Proceedings of NAVITEc, 1st ESA Workshop on Satellite Navigation User Equipment Technology*, pages 465–479. ESA, 2001.
- [21] M. Belmonte Rivas and M. Martín-Neira. GPS coherent reflections from a smooth marine surface. In *Proceedings of the 2003 Workshop on Oceanography with GNSS-R*. ESA, July 2003.
- [22] G. Ruffini, M. Caparrini, and B. Chapron. Improved ocean and em models for in-silico spaceborne GNSS-R. Technical report, PARIS Beta WP3200 - ESA ESTEC Contract No. 15083/01/NL/MM, 2001.

- [23] G. Ruffini, M. Caparrini, O. Germain, F. Soulat, and J. Lutsko. Remote sensing of the ocean by bistatic radar observations: a review. Technical report, PARIS Beta WP1000 - ESA ESTEC Contract No. 15083/01/NL/MM, 2001. Available online at <http://starlab.es>.
- [24] G. Ruffini, E. Cardellach, A. Rius, and J.M. Aparicio. Remote sensing of the ocean by bistatic observations: a review. Technical report, OPP-SCAT WP1000 - ESA ESTEC Contract 13461/99/NL/GD, 1999. Available online at <http://starlab.es>.
- [25] G. Ruffini, O. Germain, F. Soulat, M. Taani, and M. Caparrini. GNSS-R: Operational applications. In *Proceedings of the 2003 Workshop on Oceanography with GNSS-R*. Starlab, July 2003.
- [26] G. Ruffini and F. Soulat. PARIS interferometric processor analysis and experiment results, <http://arxiv.org/physics/0011027>. Technical report, IEEC and GMV - ESA Contract 14071/99/NL/MM, 2000.
- [27] G. Ruffini, F. Soulat, M. Caparrini, and O. Germain. The GNSS-R Eddy Experiment I: altimetry from low altitude aircraft. In *Proceedings of the 2003 Workshop on Oceanography with GNSS-R*. Starlab, July 2003.
- [28] V. Zavorotny and A. Voronovich. Scattering of GPS signals from the ocean with wind remote sensing application. *IEEE Trans. Geoscience and Remote Sensing*, 38(2):951–964, 2000.
- [29] C. Zuffada, R. Treuhaft, S. Lowe, G. Haij, M. Lough, L. Young, Wu S, and M. Smith. Altimetry with reflected GPS signals: results from a lakeside experiment. In *Proceedings IGARSS 2000*, 2000.

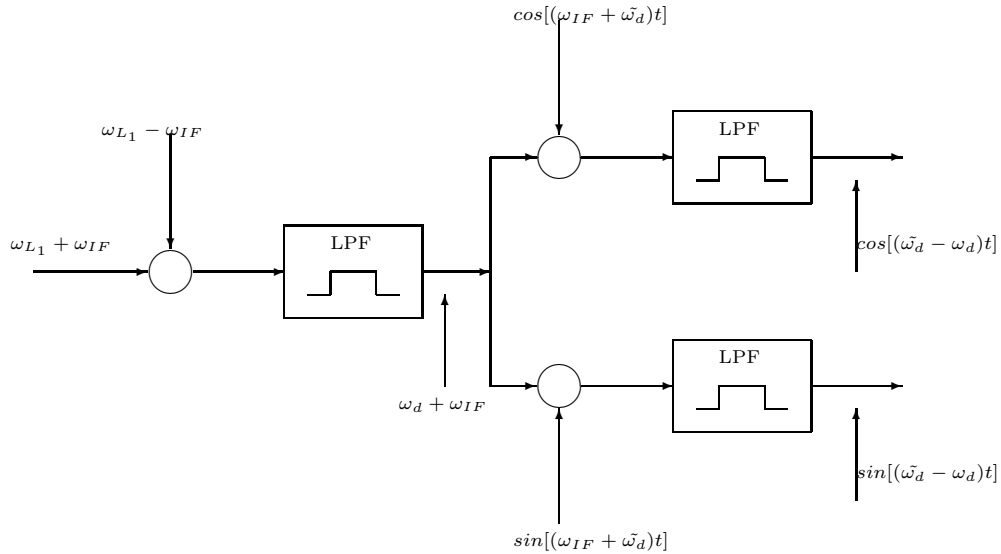


Figure 1: Starting from the in-phase component of the sampled signal, with a carrier frequency equal to the sum of the IF of the receiver and the Doppler frequency, a complex downconversion is performed. After low-pass filtering, the two obtained signals bring information about the amplitude of the backscattered EM field for both the in-phase and in-quadrature components—the spread, complex field.

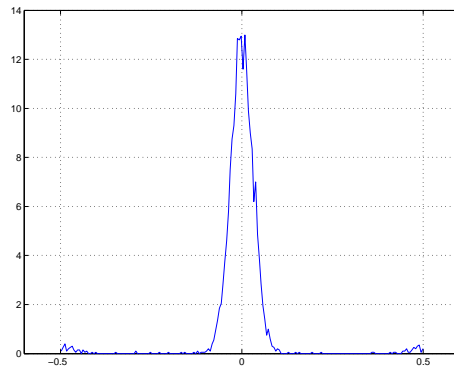


Figure 2: The histogram of the carrier phase variation, measured on an integration time interval (in this case 1 ms). The x-axis represents cycles, while on the y-axis there are arbitrary units. The accumulation of δ -phase values around zero can be seen, as well as in the vicinity of \pm half a cycle.

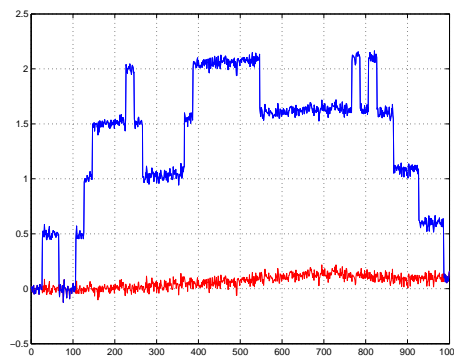
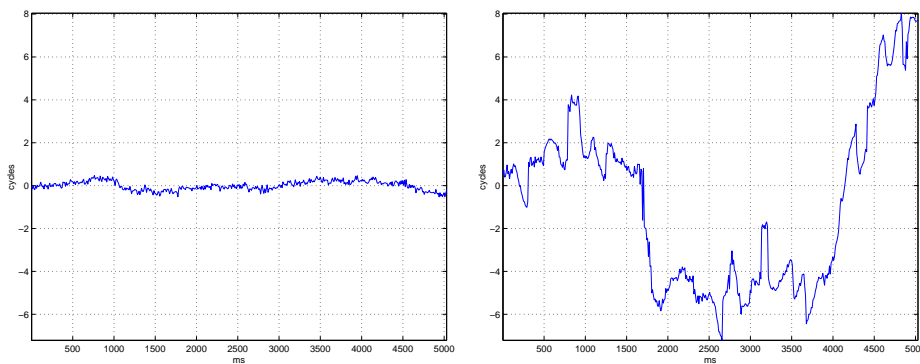


Figure 3: The direct signal carrier phase obtained accumulating the δ -phase according to Equation (5). The stepped plot represents the accumulated phase *as it is*, i.e. without compensating for the navigation bit half-cycle variation, which is clearly visible. The lower curve represents the same phase after removal of this effect (navigation bit correction). The units on the x-axis are milliseconds, and on the y-axis they are cycles.



(a) Direct field.

(b) Reflected field.

Figure 4: Example of the tracked phase, without the Doppler contribution. The units are milliseconds on the x-axis and cycles on the y axis. The integration time is 20 ms.

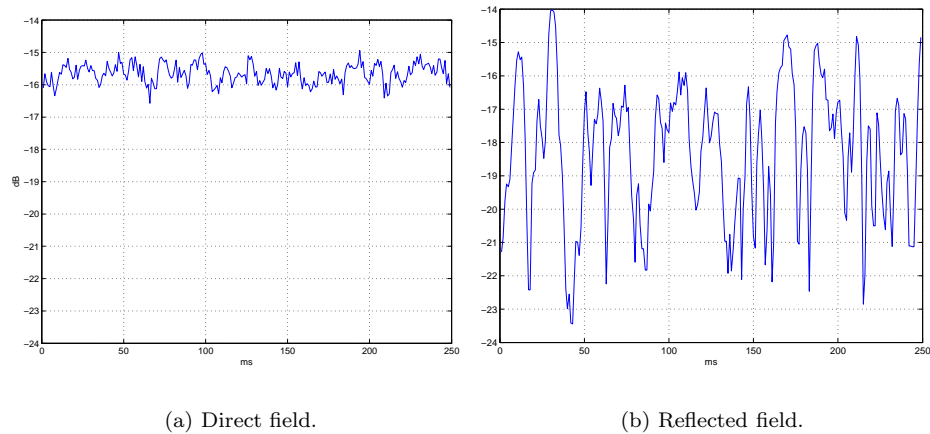


Figure 5: Example of field amplitude time series (phasor dustball, Casablanca Experiment). The units are milliseconds on the x-axis and correlation coefficient units in dB on the y axis. The integration time is 20 ms.

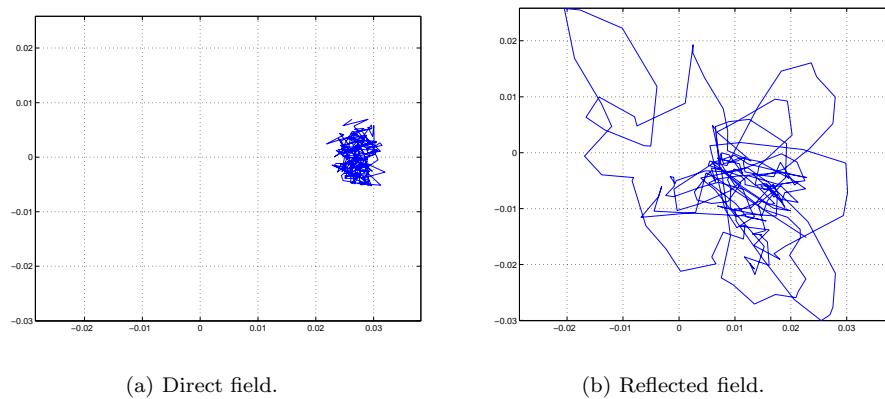


Figure 6: Example of complex field time series (phasor dustball, Casablanca Experiment). The units are correlation coefficient units on both axis. The coherent integration time is 20 ms.

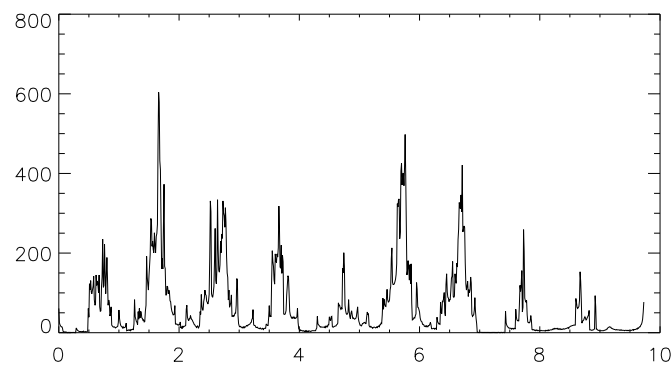


Figure 7: Histogram of the phase for a noiseless simulated field. It can be observed that the unwrapped phase wanders around multiple winding number kingdoms, while tending to spend more time around an average complex field point. This illustrates the fact that the unwrapped phase cannot be used directly for altimetry, even in the absence of noise.

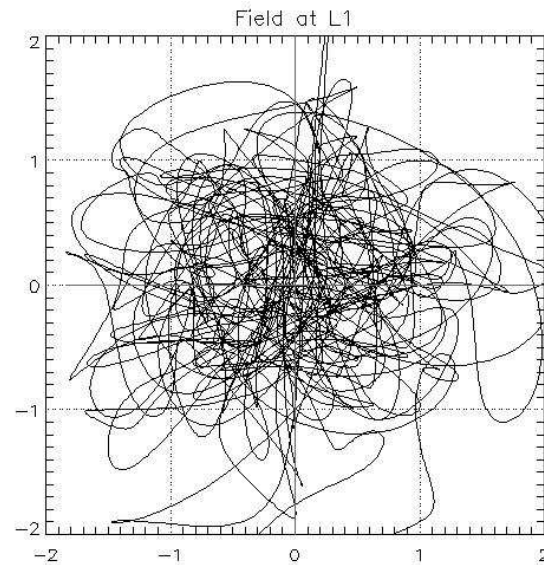


Figure 8: The simulated EM field at L1 frequency (phasor dustball), after reflection on the sea surface. The simulation has been performed with the GRADAS software [22] developed by Starlab. This simulation is for a wind speed of $U_{10} = 3$ m/s.

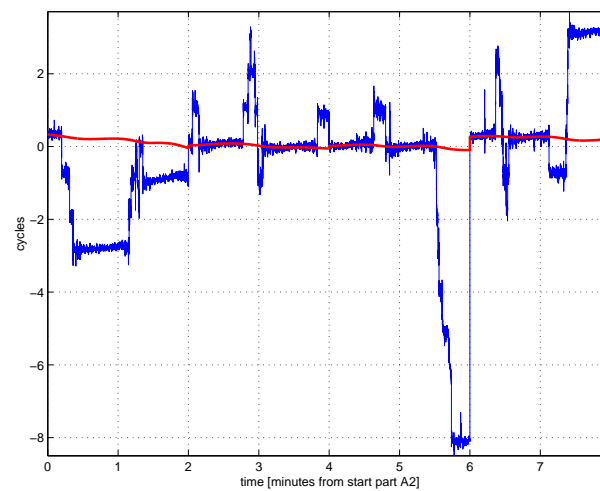


Figure 9: The blue curve is the phase of the interferometric field for PRN number 7, from minute 0 to minute 8 of Part A2 of the Bridge 2 experiment. The occurrence of a fading and of isolated cycle slips can be seen. These phenomena disappear in the phase of the filtered interferometric field (red line).

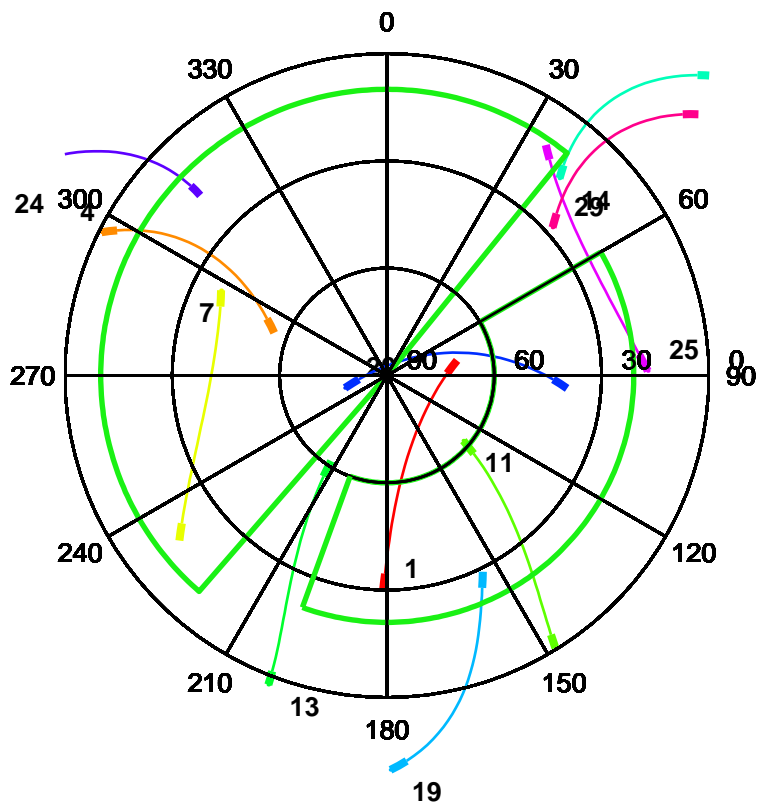
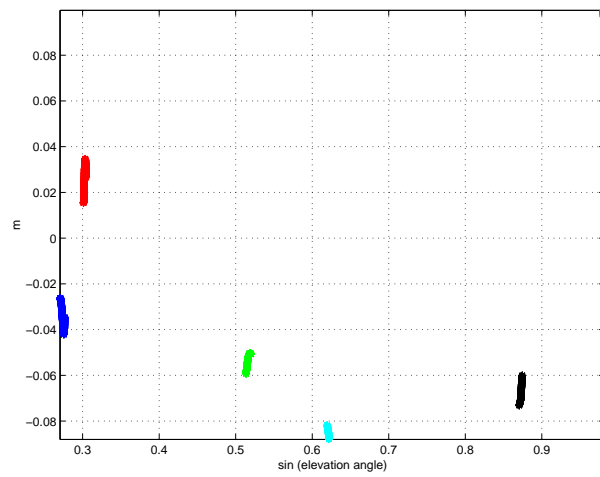
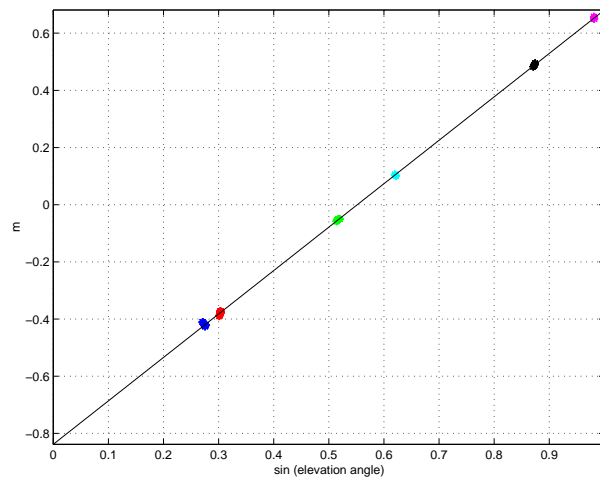


Figure 10: Each colored arc represents the position of a GPS satellite from the start of the Part A1 of the experiment to the beginning of Part A2 plus 10 minutes. The green mask represent the area where the GPS signal reflections are supposed to be free of shadowing phenomena due to the bridge structure, and therefore only the satellite within this mask can be taken into consideration for PARIS processing. The bold parts of the lines represent the first and the second 10 minutes periods.

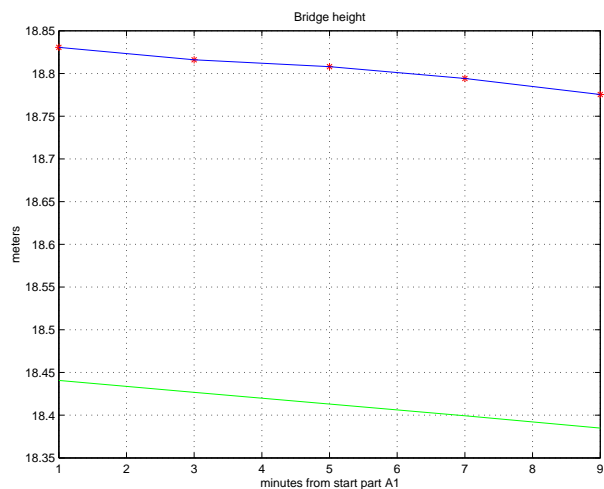


(a) In this figure, the reflected-minus-direct phase delay for each PRN is plotted with $N_P = 0$.

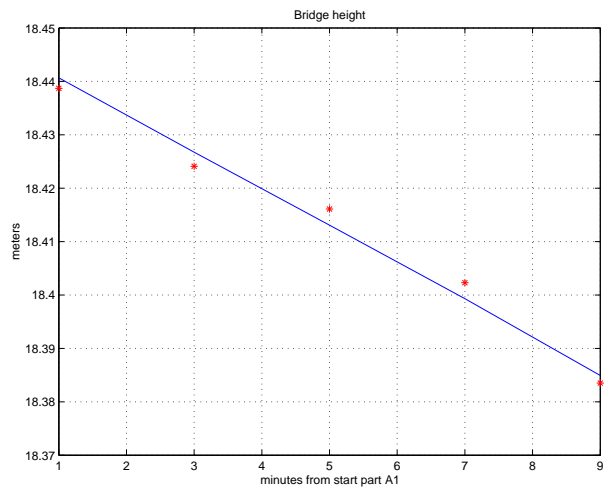


(b) In this figure, the reflected-minus-direct phase delay for each PRN is plotted with $N_P = \{001123\}$.

Figure 11: Each colored spot represents the reflected-minus-direct phase delay versus satellite-elevation for a different satellite (PRN number).

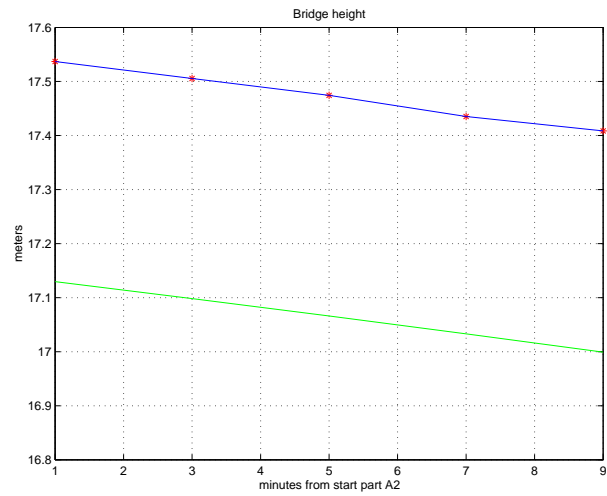


(a) The upper line is the bridge height over the water line estimated using PARFAIT. The bottom line is the bridge altitude according to the available tide measurements and the calibration of the absolute height using a GPS buoy [20].

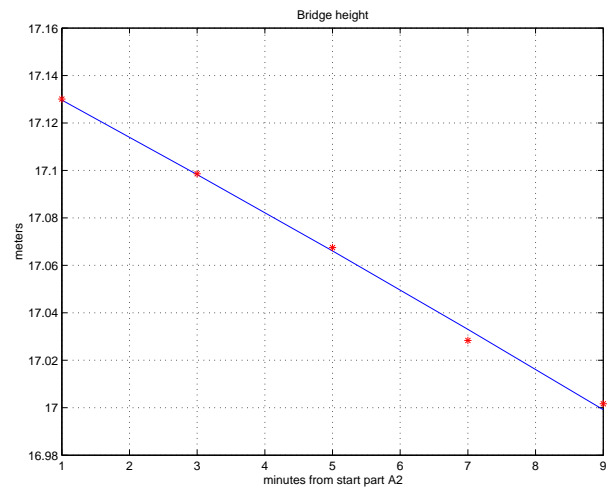


(b) In this plot, the estimates of the height (red *) and the actual height (line) are shown, after adding to the actual height the mean of the values of the last column of Table 3.

Figure 12: The bridge height estimate during the first 10 minutes of the Part A1 of the data.



(a) The upper line is the bridge height estimated using PARFAIT. The bottom line is the bridge height according to the available tide measurements and the GPS buoy measurement [20].



(b) In this plot, the estimates of the height (red *) and the actual height (line) are shown, after adding to the actual height the mean of the values of the last column of Table 4.

Figure 13: The bridge height estimation during the first 10 minutes of the Part A2 of the data.

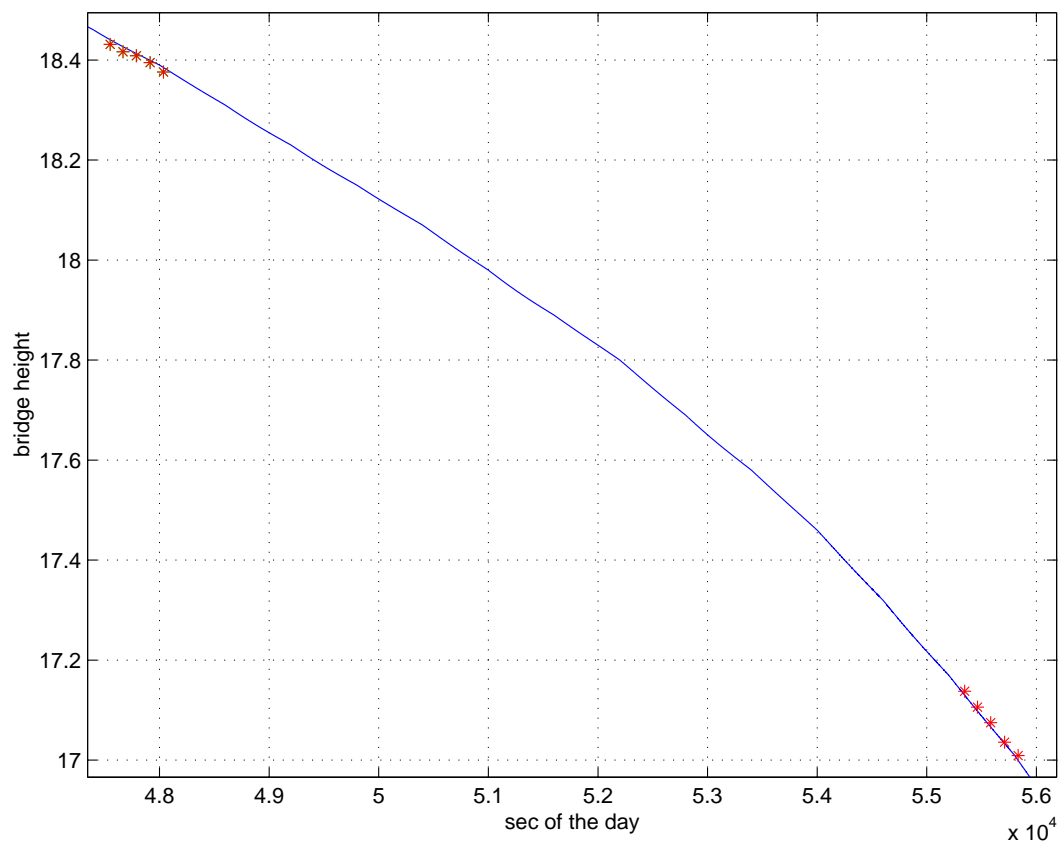


Figure 14: The solid line is the distance between the up-looking antenna and the sea surface, according to the available tide measurements and the GPS buoy measurement [20]. The green dots are the estimated values, after removing the vertical bias.